Archives available at journals.mriindia.com

International Journal of Advanced Electrical and Electronics Engineering

ISSN: 2278-8948

Volume 13 Issue 01, 2024

An IoT-Instrumented Framework for Enhancing Solar Panel Efficiency

[1]Abinesh A, [2]Ram Prakash M V, [3]Siva Sankar K, [4]Suvin S, [5]Chithra S

[1,2,3,4,5]Department of Electrical and Electronics Engineering, Stella Mary's College of Engineering, Aruthenganvilai, Kanyakumari District, Tamil Nadu 629202, India

Peer Review Information

Submission: 15 March 2024
Revision: 11 April 2024
Acceptance: 03 May 2024

Keywords

Photovoltaic Module, Solar Panel Efficiency, Internet of Things, NodeMCU, ESP8266, Blynk, Telemetry, Thermal Derating, Standard Test Conditions, Lead-Acid Battery, Remote Monitoring, Measurement Integrity.

Abstract

This paper reports the design, construction and instrumented assessment of a low-cost photovoltaic monitoring and actuation node intended to support solar-panel efficiency enhancement in residential installations. The prototype couples a PV module and a lead-acid battery to an ESP8266-based NodeMCU controller that samples panel voltage together with ambient temperature and relative humidity, drives a relay-switched DC actuator, and publishes every channel to a Blynk cloud dashboard over Wi-Fi. The telemetry actually recorded during the demonstration is reported exactly as captured: a single dashboard snapshot giving 12.29 V, 32 degrees Celsius ambient temperature and 70 % relative humidity, with the actuator in the OFF state, at one instant. Two limitations are stated openly rather than concealed. First, the dataset is a single instant on three channels, so no time series, no distribution and no uncertainty estimate can be derived from it. Second, and more consequentially, panel current was never sensed, so panel power, energy yield and any efficiency ratio, which are the very quantities the project title promises, cannot be evaluated from the recorded data, and no efficiency figure is fabricated here. The paper formalises the photovoltaic, thermal-derating and power-balance relations that the architecture presumes; adds a table of independently verifiable reference values, including the standard test conditions against which every efficiency claim is defined; and develops, under assumptions that are stated as assumptions, the thermal derating implied by the recorded 32 degrees Celsius ambient, which lies between about 10 % and 19 % of the standard-test-condition rating at full irradiance. It separates explicitly what is measured, what is computed, what is built but unmeasured, and what remains aspirational in the source design, and specifies the exact instrumentation required to convert the prototype into a quantitative efficiency study. The contribution is a disciplined, traceable path from a working but lightly instrumented teaching prototype to a deployable PV monitoring architecture.

Nomenclature

Symbol	Meaning
P_{pv}, V_{pv}, I_{pv}	PV module power (W), voltage (V) and current (A)
G, G_{STC}	Plane-of-array irradiance and its standard-test-condition value (W/m^2)
A_{pv}, η_{pv}	Module area (m^2) and conversion efficiency (%)
T_a, T_c	Ambient and cell temperature (degrees Celsius)

β	Power temperature coefficient (%/degree Celsius), negative for silicon
NOCT	Nominal operating cell temperature from the module datasheet (degrees Celsius)
RH	Relative humidity (%)
V_{oc}, I_{sc}	Open-circuit voltage (V) and short-circuit current (A)
V_{mp}, I_{mp}	Voltage and current at the maximum power point
FF, P_{max}	Fill factor and maximum module power (W)
P_{bat}, V_{bat}	Battery power (W) and terminal voltage (V)
P_{load}, P_{loss}	Load power and system loss power (W)
SoC, E_{cap}	Battery state of charge and usable capacity (Wh)
η_c, D	Charge efficiency and converter duty cycle

Introduction

Photovoltaic generation is now the fastest-growing source of new electrical capacity worldwide, and its economics are governed almost entirely by the energy a module actually delivers over its lifetime rather than by its nameplate rating [1], [2]. The gap between nameplate and delivered energy is opened by effects that are all, in principle, observable: cell heating, soiling, partial shading, mismatch, and the operating point imposed by the load or the charge controller [3], [4]. That observability is what makes low-cost instrumentation attractive. If a module's electrical output and its thermal environment are sampled continuously and published to a network, the losses can be attributed rather than guessed, and corrective action such as cleaning, cooling, reorientation or a change of operating point can be triggered automatically.

The Internet of Things has made such instrumentation inexpensive. A Wi-Fi-enabled microcontroller costing a few dollars can sample analogue channels, drive actuators through relays and stream data to a cloud dashboard without any bespoke networking effort [8], [9]. This paper reports a prototype of exactly that kind, built around a NodeMCU (ESP8266) node, a PV module, a lead-acid battery, a relay-driven DC actuator and the Blynk platform. The paper treats the build as a measurement campaign and is deliberately explicit about what the campaign's output can and cannot support. That discipline is the paper's defining feature, because the recorded telemetry is considerably narrower than the project's stated ambition.

1. Problem Statement

Undergraduate and teaching-scale PV monitoring projects are numerous, and they almost universally report that a dashboard works, in the sense that values appear on a phone, without reporting the electrical quantity the monitoring exists to serve. Efficiency is named in the title, defined in the text, and then never evaluated, because current is not sensed. Meanwhile, system-level PV performance studies assume fully instrumented modules with pyranometers and calibrated shunts. There is little work that carries one transparently reported, and admittedly narrow, prototype dataset through to an architecture proposal while separating measured fact, unmeasured capability and aspiration.

2. Objectives

The specific objectives of the work are as follows:

- To build a low-cost IoT node that senses panel-side voltage, ambient temperature and relative humidity, drives a relay-switched actuator, and publishes every channel to a cloud dashboard.
- To report the telemetry exactly as captured, with the sampling instant, the channel full scales and the actuator state stated.
- To establish precisely why module efficiency cannot be evaluated from that telemetry, and which sensor is missing.
- To consolidate the governing photovoltaic, fill-factor, thermal-derating and power-balance relations that the architecture presumes.
- To quantify, under assumptions that are labelled as assumptions, the thermal derating implied by the recorded ambient conditions, so that the magnitude of the effect is at least bounded.
- To separate the source design into subsystems that were built and measured, built but unmeasured, and proposed but not implemented, and to specify the measurement plan that would close the gap.

3. Scope and Delimitation

The study covers the construction of the node, the relations governing photovoltaic output, the reading of the single recorded snapshot, and the specification of the instrumentation that was absent. It explicitly excludes any claim of module efficiency, panel power, energy yield, performance ratio or actuator benefit, because none of these can be evaluated from the recorded channels. It also excludes the advanced subsystems named in the source design documentation, which were not built. Every figure drawn from the literature, and every value derived from an assumption rather than a measurement, is labelled as such at the point of use.

4. Contributions

1. A transparent report of the telemetry actually captured by the prototype, with the sampling instant, channel full scales and actuator state stated.
2. A precise statement of why module efficiency cannot be evaluated from that telemetry, and exactly which sensor is missing.
3. A consolidated set of governing relations covering photovoltaic output, efficiency, fill factor, thermal derating and DC power balance.
4. An assumption-based derating analysis, new to this revision, which bounds the thermal loss implied by the recorded 32 degrees Celsius ambient at between roughly 10 % and 19 % at full irradiance, and states every assumption used to obtain it.
5. A table of independently verifiable reference values, including the definition of standard test conditions and current record silicon efficiencies, so that the meaning of an efficiency claim is fixed before any claim is made.
6. A separation of the source design into subsystems that were built and measured, built but unmeasured, and proposed but not implemented, with a measurement plan that would close the gap.

The remainder of the paper is organised as follows. Section II reviews related work and fixes the reference values. Section III gives the governing relations. Section IV describes the prototype and the method. Section V reports the recorded data and its honest reading. Section VI discusses the findings, Section VII states the limitations, and Section VIII proposes the monitoring and enhancement framework. Sections IX and X give the conclusion and the future scope.

Related Work

Green and colleagues [1] maintain the reference efficiency tables against which any module claim must ultimately be compared, and their methodology notes make plain that an efficiency statement is meaningless without simultaneous irradiance, temperature and full current-voltage characterisation. Skoplaki and Palyvos [3] reviewed the operating-temperature dependence of photovoltaic electrical performance and consolidated the linear derating model used in Section III; the coefficient β is technology-dependent and must be taken from the module datasheet or measured, never assumed.

On soiling and cleaning, which is one plausible function of a relay-driven actuator in a photovoltaic context, Sarver, Al-Qaraghuli and Kazmerski [4] surveyed mitigation techniques and reported that losses depend strongly on local dust deposition rates, so cleaning benefit is site-specific and cannot be transferred between installations. For the conversion and storage stage, Dunlop and Farhi [5] documented lead-acid behaviour in stand-alone photovoltaic service, including the charge-voltage limits that a controller must respect. On the instrumentation side, Adhya and colleagues [6] and Priharti and colleagues [7] describe IoT-based photovoltaic monitoring nodes; the latter senses both voltage and current, and only then does the node report power. That single difference is the one that separates their work from the present prototype. Espressif's ESP8266 platform [8] and the Blynk framework [9] supply the networking and visualisation layers used here.

Table 1. Representative Related Work and its Relation to This Study

Ref.	Year	Focus and scope	Method and validation	Relation to this work
[1]	2023-	Reference PV efficiency tables	Certified laboratory current-voltage measurement	Defines what an efficiency claim requires
[3]	2009	Operating temperature versus electrical yield	Review; linear derating correlations	Source of the derating model, Eq. (4)
[4]	2013	Soiling losses and mitigation	Review of field studies	Motivates the actuator; benefit is site-specific
[5]	1997	Lead-acid batteries in stand-alone PV	Handbook; field practice	Charge-limit basis for the storage stage

[6]	2016	IoT-based PV monitoring node	Prototype; cloud dashboard	Closest comparable architecture
[7]	2019	Wireless PV performance monitoring	Prototype with voltage and current sensing	Shows the sensor this prototype lacks
[8]	—	ESP8266 system-on-chip platform	Vendor documentation	Controller and Wi-Fi stack
[9]	—	Blynk IoT platform	Vendor documentation	Dashboard and virtual-pin transport
[11]	2019	IEC 60904-3 measurement principles	International standard	Fixes the definition of standard test conditions
[12]	2026	Solar cell efficiency tables, Version 67	Independently confirmed measurement	Current record efficiencies, Table II
[13]	2026	Fraunhofer ISE Photovoltaics Report	Industry data compilation	Technology mix context, Table II

The year for [4] is given as 2013, the publication year of the cited review by Sarver and colleagues. An earlier draft of this work carried 2016 and a different author name for the same reference; the entry has been corrected against the reference list.

Because the present paper turns on the difference between a measured quantity and a quoted one, it is useful to fix a small set of reference values that can be checked against primary sources. These are collected in Table 2. None is a measurement of this prototype; they establish the frame within which any efficiency statement would have to be made.

Table 2. Independently Verifiable Reference Values

Item	Value	Source
Standard test conditions	1000 W/m² irradiance, 25 degrees Celsius cell temperature, AM1.5 reference spectrum	IEC 60904-3 [11]
NOCT reference environment	800 W/m², 20 degrees Celsius ambient, 1 m/s wind speed	Standard practice [11]
Typical field cell temperature	45 to 65 degrees Celsius in normal outdoor operation	Industry practice [3]
Record silicon cell efficiency	27.9 % masked; 27.7 % on a total-area basis	Efficiency tables, Version 67 [12]
Silicon share of module production, 2025	About 98 % of production; 86 % n-type wafers	Fraunhofer ISE report [13]
Silicon power temperature coefficient	−0.3 to −0.5 %/degree Celsius, technology-dependent	Datasheet range [3]
Lead-acid charge-voltage limit	About 14.4 V at 20 degrees Celsius for a 12 V battery	Device specification [5]

Values are published figures and standard definitions. They are given so that the reader can see what an efficiency claim would have to be measured against. No value in this table was measured on the hardware described in Section IV.

System Modelling

1. Photovoltaic Output and Efficiency

The electrical power delivered by a photovoltaic module at any instant is the product of its terminal quantities,

$$P_{pv} = V_{pv} I_{pv} \qquad (1)$$

and its conversion efficiency is that power referred to the solar power incident on the module aperture,

$$\eta_{pv} = \frac{P_{pv}}{GA_{pv}} \times 100\,\% = \frac{V_{pv} I_{pv}}{GA_{pv}} \times 100\,\% \qquad (2)$$

Equations (1) and (2) are the reason the present dataset is insufficient, and this is developed in Section V-C. Both require a current measurement; the second additionally requires an irradiance measurement and the module aperture area.

2. Fill Factor

The shape of the module characteristic is captured by the fill factor,

$$FF = \frac{V_{mp} I_{mp}}{V_{oc} I_{sc}}, \qquad P_{max} = FF\, V_{oc} I_{sc} \qquad (3)$$

where V_{mp} and I_{mp} are the voltage and current at the maximum power point. A representative current-voltage and power-voltage pair is shown in Fig. 1. It is drawn from the model, not measured here, and is labelled as such in the figure itself.

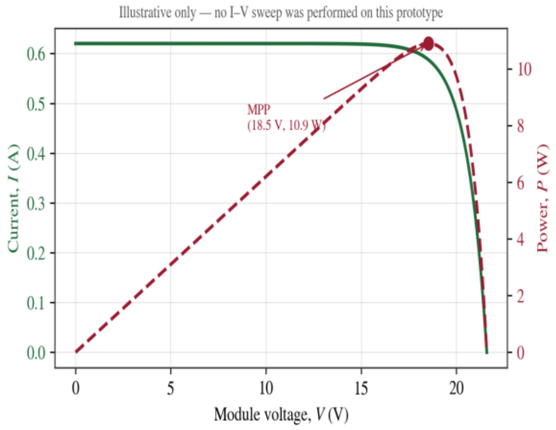

Figure 1: Illustrative module current-voltage and power-voltage characteristics with the maximum power point marked. No current-voltage sweep was performed on this prototype, so no point on these curves is a measurement of it.

3. Thermal Derating

Cell temperature depresses output approximately linearly about the standard-test-condition value [3],

$$P_{pv}(T_c) = P_{STC}\frac{G}{G_{STC}}[1+\beta(T_c-25)] \qquad (4)$$

with β negative and typically between −0.3 and −0.5 %/degree Celsius for crystalline silicon. Cell temperature exceeds ambient under irradiance; a widely used first-order estimate is

$$T_c \approx T_a + \frac{NOCT-20}{800}G \qquad (5)$$

where NOCT is the nominal operating cell temperature from the module datasheet, defined for an open-rack module at 800 W/m^2, 20 degrees Celsius ambient and 1 m/s wind [11]. Fig. 2 shows the family of derating lines implied by Eq. (4). The lines are illustrative, since neither β nor G was available for this prototype.

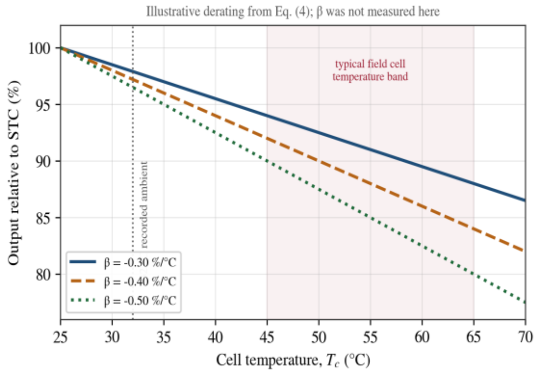

Figure 2: Illustrative thermal derating from Eq. (4) for three values of β, with the recorded ambient temperature and the typical field cell-temperature band marked for orientation only.

4. DC Power Balance and Storage

At the DC node the powers balance as

$$P_{pv} = P_{load} + P_{bat} + P_{loss} \qquad (6)$$

where P_{bat} is positive when charging, and the battery state of charge evolves as

$$SoC(t+\Delta t) = SoC(t) + \frac{\eta_c P_{bat}(t)\,\Delta t}{E_{cap}} \qquad (7)$$

Neither relation can be evaluated for the present build, because no current is sensed at any node in the chain.

Prototype and Methodology

1. Architecture

Fig. 3 shows the prototype. The node samples panel voltage through a resistive divider and ambient temperature and relative humidity through a digital temperature-humidity sensor, drives a DC actuator through a relay module, and maintains a Wi-Fi session with the Blynk cloud so that all channels appear on a mobile dashboard and the actuator can be commanded remotely. The three channels required to close Eqs. (1) and (2), namely panel current, plane-of-array irradiance and time-stamped logging, are shown in the figure as absent, because that is what they are.

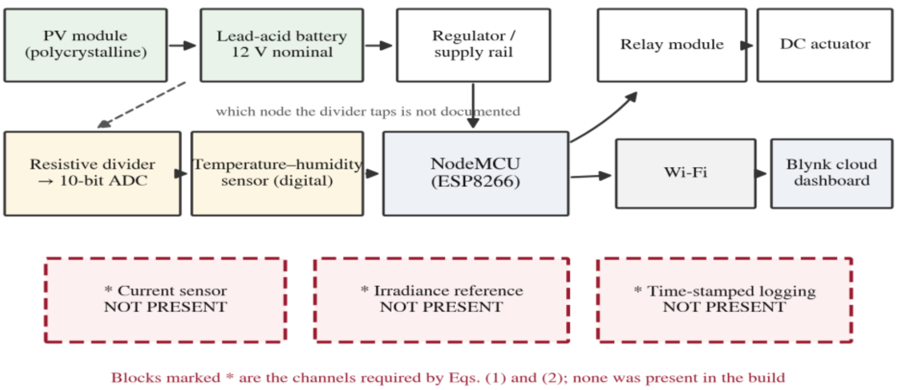

Fig. 3: Prototype architecture. Voltage, temperature and humidity are sensed; panel current, irradiance and time-stamped logging are not.

2. Apparatus

Table 3 lists the apparatus. Component ratings are stated only where the source documentation states them; blanks are left where it does not, rather than filled with plausible values.

Table 3. Apparatus Used in the Prototype

Item	Type / rating	Quantity
PV module	Polycrystalline; rating not stated in the record	1
Storage battery	Lead-acid, 12 V nominal	1
Controller board	NodeMCU (ESP8266)	1
Temperature-humidity sensor	Digital, single-wire	1
Voltage sensing	Resistive divider to the controller ADC	1
Relay module	Rating not stated in the record	1
DC actuator	Type not stated in the record	1
Dashboard	Blynk (cloud)	1
Connecting wires	—	as required

The module nameplate power, aperture area, open-circuit voltage, temperature coefficient and NOCT are not recorded. Their absence is a second reason, independent of the missing current sensor, why no efficiency figure can be produced.

3. Procedure

- Assemble the chain from PV module through battery and regulator to the NodeMCU, and wire the sensor, relay and actuator to the controller's general-purpose pins.
- Flash the node from the Arduino IDE with the Blynk library, binding each channel to a virtual pin and the actuator to a dashboard switch.
- Bring the node online, confirm that the device appears on the dashboard, and record the displayed channel values and the actuator state.

4. Measurement Resolution of the Voltage Channel

The ESP8266 provides a single 10-bit analogue-to-digital converter [8]. If the resistive divider is scaled so that the dashboard's 0 to 15 V gauge spans the converter's full input range, the quantisation step is 15 V divided by 1024, or about 14.7 mV per least significant bit. This figure is computed from the stated gauge full scale and the converter word length; it is not a measured accuracy, and it excludes divider tolerance, reference-voltage error and noise, all of which are larger contributors in a build of this kind. It is quoted only to show that the recorded resolution is not the limiting problem. The limiting problem is the absent channel, not the precision of the present one.

Results

1. Recorded Telemetry

Table 4 reports the telemetry exactly as captured from the dashboard. All three values belong to one instant. The device identifier and the clock reading shown on the dashboard are included so that the record is traceable. Fig. 4 presents the same three values as a fraction of their gauge full scale.

Table 4. Recorded Dashboard Telemetry (Single Snapshot)

Channel	Value	Gauge full scale	Status
Panel voltage	12.29 V	0 to 15 V	measured
Ambient temperature	32 degrees Celsius	0 to 100	measured
Relative humidity	70 %	0 to 100 %	measured
Actuator state	OFF	—	observed
Sampling instant	11:37	—	observed
Device identifier	solar FE8CC	—	observed

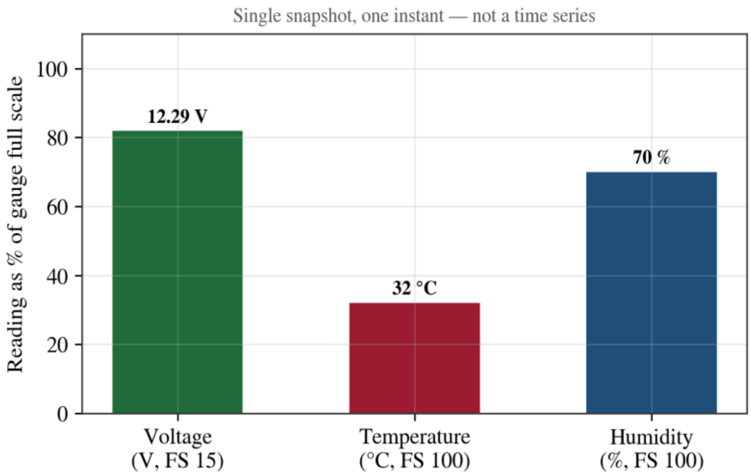

Figure 4: Recorded channels expressed as a fraction of their dashboard full scale. The plot contains one sample per channel and therefore shows no trend; it is a snapshot rendered as bars and must not be read as a time series.

2. An Honest Reading of the Data

Three features of this dataset must be stated plainly.

It is a single instant. One sample per channel supports no mean, no variance, no trend and no uncertainty estimate. Nothing in this paper treats these three numbers as a distribution.

The recorded voltage is consistent with a charged 12 V lead-acid battery, not with an illuminated module at its maximum power point. A 12 V nominal lead-acid battery rests near 12.6 to 12.8 V and sits between roughly 12.0 and 12.4 V under light load, whereas a 12 V-class photovoltaic module has an open-circuit voltage of about 21 V and operates near 17 V at the maximum power point. The recorded 12.29 V therefore most plausibly reports the battery-side node rather than the module terminals. The source documentation does not state which node the divider is connected to, so this reading is offered as the most consistent interpretation and is flagged as an inference, not as a fact.

The ambient conditions were warm and humid. An ambient of 32 degrees Celsius with 70 % relative humidity implies, by Eq. (5), a cell temperature well above ambient under any appreciable irradiance, and hence a material derating by Eq. (4). The magnitude of that derating cannot be measured here, but it can be bounded under stated assumptions, and Section V-D does so.

3. Why Panel Efficiency Cannot Be Computed Here

The efficiency the project sets out to enhance is defined by Eq. (2) and requires three quantities: panel voltage, panel current and incident irradiance, together with the module area. The prototype senses only voltage. No current sensor is present in the build, and no irradiance reference was deployed. Consequently:

- P_{pv} cannot be evaluated, because Eq. (1) requires I_{pv}.
- η_{pv} cannot be evaluated, because Eq. (2) requires both I_{pv} and G, and additionally the module aperture area, which the record does not state.
- Energy yield cannot be evaluated, because power is unavailable and the samples are not time-stamped as a series.
- The effect of the actuator cannot be quantified, because no paired before-and-after measurement of any electrical quantity was taken.

No efficiency value is therefore reported. To indicate the leverage of the missing channel rather than to supply a result: with the recorded 12.29 V held fixed, a panel current anywhere in the range 0.2 to 1.0 A would place panel power between about 2.5 and 12.3 W. The spread is a factor of five, and the whole of it is unresolved by the present instrumentation. That single sentence is the case for a current sensor.

4. Thermal Derating Implied by the Recorded Ambient

Although β and G were not measured, the recorded ambient temperature is a genuine measurement, and it can be propagated through Eqs. (5) and (4) under assumptions that are declared. Taking NOCT as 45 degrees Celsius, which is a common datasheet value for crystalline silicon and is used here as an assumption rather than a specification of this module, the thermal loss relative to standard test conditions is

$$\Delta P[\%] = |\beta|(T_c - 25) \quad (9)$$

Table 5 evaluates this for three irradiance levels and the three ends of the coefficient range in Table 2. Fig. 5 plots the same relation continuously.

Table 5. Thermal Loss Implied by the Recorded 32 Degrees Celsius Ambient (Computed Under Stated Assumptions, Not Measured)

Assumed irradiance	Implied T_c, Eq. (5)	Loss at β = −0.3	Loss at β = −0.4	Loss at β = −0.5
600 W/m^2	50.8 degrees C	7.7 %	10.3 %	12.9 %
800 W/m^2	57.0 degrees C	9.6 %	12.8 %	16.0 %
1000 W/m^2	63.3 degrees C	11.5 %	15.3 %	19.1 %

Assumptions: ambient 32 degrees Celsius as recorded; NOCT taken as 45 degrees Celsius; β taken across the datasheet range of Table II; open-rack mounting and the first-order model of Eq. (5). None of these was measured on this prototype, and the module's own NOCT and β are not documented. The table bounds the magnitude of an effect; it is not a performance result.

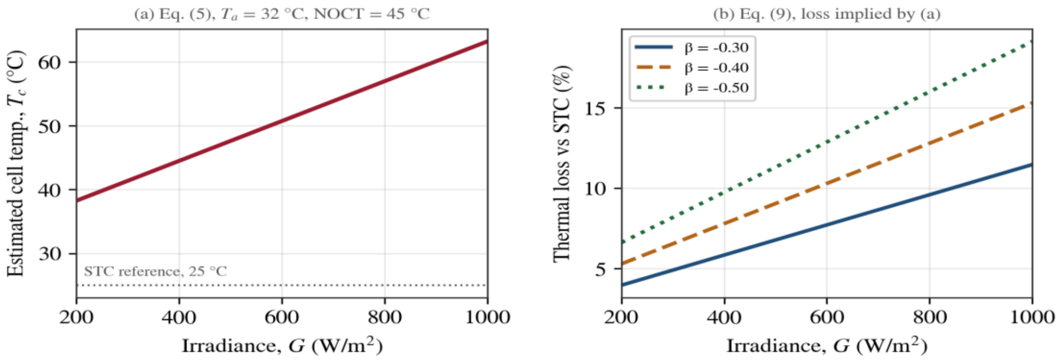

Figure 5: (a) Cell temperature implied by Eq. (5) for the recorded 32 degrees Celsius ambient and an assumed NOCT of 45 degrees Celsius; (b) the thermal loss that follows from Eq. (9) for three values of β.

The practical reading is that at this site, on this day, thermal derating of order ten to twenty per cent was probably present and entirely invisible to the instrumentation. A monitoring node that reports 32 degrees Celsius but cannot report the power that temperature is suppressing is displaying the cause without the effect.

5. What the Prototype Supports

Table 6 states the position quantity by quantity. As in the previous section, the entries that were not obtained outnumber those that were, and that asymmetry is the honest summary of the campaign.

Table 6. Measured, Built, Documented and Indeterminate Quantities

Quantity or capability	Value	Status
Panel or battery-node voltage	12.29 V	measured
Ambient temperature	32 degrees Celsius	measured
Relative humidity	70 %	measured
Sampling instant	11:37, single instant	observed
Remote actuator command	OFF	built, exercised
Thermal loss at 32 degrees Celsius ambient	about 10 to 19 % at full irradiance	computed under assumptions, Eq. (9)
Voltage-channel quantisation step	about 14.7 mV per LSB	computed from [8] and gauge full scale

Discussion

The prototype establishes that a low-cost node can sense a small set of environmental and electrical channels, publish them reliably to a cloud dashboard, and accept a remote command. That is a real result and it is not diminished by what follows. What the prototype does not establish is anything about efficiency, which is the quantity its title names. The distinction matters because the two are routinely conflated in reports of this kind, and the conflation is what turns a working teaching prototype into an unsupported performance claim.

1. Scope Note on the Source Design

The design documentation accompanying this prototype describes bifacial modules with dynamic tracking, nanostructured coatings, tandem silicon-perovskite cells, hydrogen storage and artificial-intelligence optimisation. None of these appears in the constructed hardware, which is a single fixed module, a lead-acid battery, a microcontroller, a relay and an actuator. They are recorded here as design aspirations for a future system and are excluded from every result, table and claim in this paper. Conflating an aspiration with a built subsystem is the most common failure mode in reports of this kind, and it is avoided deliberately.

2. The Reference Frame for an Efficiency Claim

Table 2 makes the scale of the gap concrete. An efficiency figure is defined at standard test conditions, that is at 1000 W/m² and a cell temperature of 25 degrees Celsius under the AM1.5 spectrum [11], a combination that does not occur on a roof. Certified record silicon cells now reach 27.9 % under those conditions [12], and silicon accounts for the overwhelming majority of module production [13]. A prototype that reports neither irradiance nor current is not merely less precise than that frame; it is outside it altogether, because it produces no quantity of the same kind. Recognising this is what makes the measurement plan of Section VIII specific rather than aspirational.

3. Qualitative Position

Table 7 sets out the properties that can be asserted, each with the relation or source that supports it.

Table 7. Qualitative Benefits of the Proposed Framework and Their Basis

Feature	Benefit	Basis
Current sensing	Makes P_{pv} and η_{pv} computable	Eqs. (1), (2)
Irradiance reference	Separates resource variation from system fault	[1], [11]
Thermal monitoring	Predicts derating; flags abnormal heating	[3], Eq. (4)
MPP control	Chooses the operating point instead of inheriting it	Eq. (8)
Condition-based cleaning	Triggers on evidence; benefit becomes measurable	[4]
Time-stamped logging	Enables energy yield and performance ratio	Eqs. (1), (2) over time
Cloud dashboard	Remote visibility and command (demonstrated)	This work

Limitations

The following limitations bound every claim made in this paper.

- The dataset is one sample on three channels at one instant. No statistical quantity of any kind can be derived from it.
- Panel current was never sensed. Panel power, efficiency, energy yield and performance ratio are therefore indeterminate for this build, not merely uncertain.
- No irradiance reference was deployed, so the denominator of Eq. (2) is unavailable even if current were known.
- The module's nameplate rating, aperture area, temperature coefficient and NOCT are not documented, so the derating analysis of Section V-D rests on assumed rather than specified values and bounds an effect rather than measuring one.
- The node to which the resistive divider is connected is not documented. The battery-side interpretation of the recorded 12.29 V is an inference from plausible operating voltages, not an established fact.
- The actuator was exercised but its effect was never measured, because no paired electrical measurement was taken before and after actuation.
- The quantisation figure of about 14.7 mV per least significant bit is a computed resolution, not a measured accuracy; divider tolerance, reference error and noise are not characterised.
- Figures 1 and 2 are illustrative plots of the governing relations and contain no data point from this hardware.
- The advanced subsystems described in the source design documentation were not built and are excluded from every claim.

Proposed Monitoring and Enhancement Framework

The measured chain motivates the architecture of Fig. 6, in which the sensing layer is completed, a decision layer attributes losses, and an actuation layer responds. The fast inner loop is operating-point control; the slow outer loop is condition-based actuation.

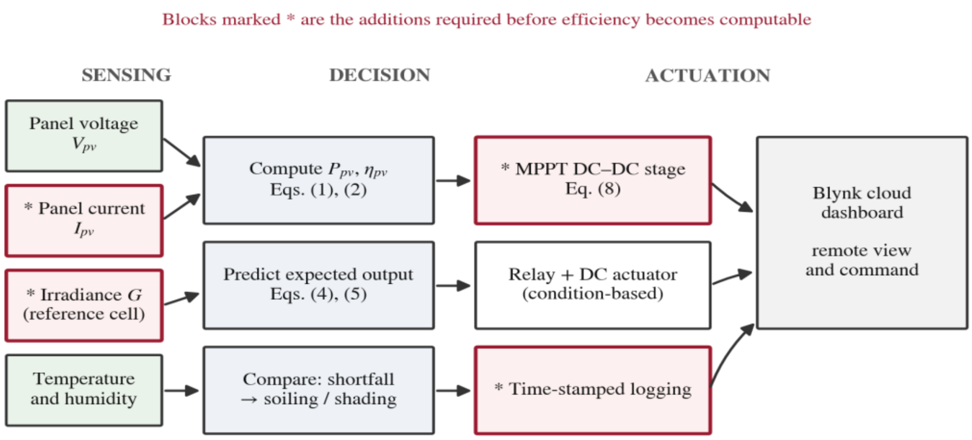

Figure 6: Proposed framework. Channels marked with an asterisk are the additions required to make efficiency computable; all others exist in the present prototype.

1. Completing the Sensing Layer

A Hall-effect or shunt-based current sensor placed in the module lead makes P_{pv} available through Eq. (1) at no change to the controller architecture. A calibrated reference cell or pyranometer makes η_{pv} available through Eq. (2). These two additions convert the node from a status display into a performance instrument, and they are the single highest-value change to the present build. Logging the measured parameters continuously then allows performance to be evaluated under changing irradiance and temperature, which supports the identification of losses and timely maintenance or controller optimisation.

2. Operating-Point Control

With current available, a perturb-and-observe controller can hold the module near its maximum power point by perturbing a converter duty cycle D and observing the sign of the resulting change in power:

$$D(k+1) = D(k) + \Delta D \ (\Delta P/\Delta D > 0); \ D(k) - \Delta D \ (\Delta P/\Delta D < 0) \tag{8}$$

The present prototype has no such converter. The module is tied to the battery node, so the operating point is imposed by battery voltage rather than chosen. This is a structural limitation of the build, not a tuning issue, and it is a second reason why the recorded voltage sits near battery potential rather than near a module maximum power point.

3. Condition-Based Actuation

Once power is observable, actuation can be triggered on evidence rather than on a timer. A persistent shortfall of measured power against the power predicted by Eqs. (4) and (5) from the measured irradiance and temperature indicates soiling or shading, and is the correct trigger for a cleaning cycle. The benefit of each cycle is then measurable as the recovered power, which is precisely the quantity the present prototype cannot see.

4. Illustrative Figures and Measurement Plan

Table 8 gives an illustrative benefit sketch whose entries are explicitly literature ranges or device specifications, not measurements and not guarantees. Table 9 sets out the measurement plan that would make the assessment quantitative.

Table 8. Illustrative Figures (Assumptions and Specifications, Not Results)

Item	Illustrative value	Status
Silicon power temperature coefficient	−0.3 to −0.5 %/degree Celsius	datasheet range [3]
Soiling loss	Wide and site-specific	literature [4]
Lead-acid charge limit	14.4 V at 20 degrees Celsius for 12 V	device specification [5]
Assumed NOCT used in Section V-D	45 degrees Celsius	assumption, not this module
Assumed consumption of the analysis	—	no load profile was recorded
Measured module efficiency	—	indeterminate

Values are literature ranges or device specifications included to indicate order of magnitude only. They were not measured in this work and must not be read as performance guarantees.

Table 9. Measurement Plan Required to Make the Assessment Quantitative

Measurement	Instrument or method	Quantity it yields
Panel current	Hall-effect or shunt sensor in the module lead	I_{pv}, and hence P_{pv} by Eq. (1)
Plane-of-array irradiance	Calibrated reference cell or pyranometer	G, and hence η_{pv} by Eq. (2)
Module characterisation	Datasheet capture and verification	A_{pv}, nameplate rating, β and NOCT
Time-series logging	Fixed-interval sampling with time stamps across whole days	Daily energy, capacity factor, performance ratio
Sensing-node resolution	Continuity check and dual instrumentation of both nodes	Removes the 12.29 V ambiguity of Section V-B
Actuator quantification	Paired before-and-after trials under logged irradiance and temperature	Recovered power attributable to actuation
Operating-point control	DC-DC stage under Eq. (8)	Controlled rather than imposed operating point
Channel accuracy	Calibration of the divider against a reference meter	Measured accuracy, not merely quantisation

Conclusion

A low-cost IoT node for photovoltaic monitoring and actuation was built and exercised. The node reliably sensed panel-side voltage, ambient temperature and relative humidity, published them to a cloud dashboard, and accepted a remote actuator command. The recorded snapshot was 12.29 V, 32 degrees Celsius and 70 % relative humidity with the actuator OFF, at a single instant.

The recorded voltage was shown to be more consistent with a battery-side node than with an illuminated module at its maximum power point, and this interpretation was flagged as an inference rather than a fact. Because panel current was never sensed and no irradiance reference was deployed, panel power, energy yield and the module efficiency named in the project's own title cannot be computed from the recorded data, and no efficiency value was fabricated. The measured, built-but-unmeasured, and merely aspirational parts of the design were separated explicitly in Table VI.

The governing photovoltaic, derating, fill-factor and power-balance relations were consolidated, and the recorded ambient temperature was propagated through them under declared assumptions to bound the thermal loss at roughly 10 to 19 % of the standard-test-condition rating at full irradiance. That figure is a bound obtained from an assumption set, not a measurement, and it is labelled as such wherever it appears; its purpose is to show that the effect the node can see the cause of is large enough to matter. A framework was then proposed in which two additional sensors, current and irradiance, convert the existing node from a status display into a performance instrument.

The paper's value lies in its traceable path from a modest, honestly reported prototype dataset to a deployable photovoltaic monitoring architecture, and in the concrete measurement plan of Table IX required to make the assessment quantitative.

Future Work

Several extensions follow directly from the limitations above.

- Add current sensing-Install a Hall-effect or shunt current sensor in the module lead so that P_{pv}, and hence η_{pv}, become real results rather than symbols.
- Add an irradiance reference-Deploy a calibrated reference cell or pyranometer in the plane of array so that Eq. (2) closes.
- Log time series, not snapshots-Record all channels at a fixed interval with time stamps across whole days, so that daily energy, capacity factor and performance ratio can be computed.
- Resolve the sensing node-Document and verify whether the divider reads module or battery terminals, and instrument both, so that the 12.29 V ambiguity identified in Section V-B does not recur.
- Capture the module datasheet-Record the nameplate rating, aperture area, temperature coefficient and NOCT, so that the derating analysis of Section V-D can be repeated with specified rather than assumed values.
- Quantify the actuator-Run paired before-and-after trials of the actuator under logged irradiance and temperature, so that its benefit is measured rather than asserted.
- Add maximum-power-point conversion-Insert a DC-DC stage under Eq. (8) so that the operating point is controlled rather than imposed by the battery.

Acknowledgment

The authors thank the Department of Electrical and Electronics Engineering, Stella Mary's College of Engineering, for laboratory facilities and guidance during the project.

References

M. A. Green et al., "Solar cell efficiency tables," Progress in Photovoltaics: Research and Applications, published in successive versions, Wiley.

T. Townsend and C. Whitaker, "Measured vs. rated PV system performance," in Proc. IEEE Photovoltaic Specialists Conference.

E. Skoplaki and J. A. Palyvos, "On the temperature dependence of photovoltaic module electrical performance: A review of efficiency/power correlations," Solar Energy, vol. 83, no. 5, pp. 614-624, 2009.

T. Sarver, A. Al-Qaraghuli, and L. L. Kazmerski, "A comprehensive review of the impact of dust on the use of solar energy," Renewable and Sustainable Energy Reviews, vol. 22, pp. 698-733, 2013.

J. P. Dunlop and B. N. Farhi, "Recommendations for maximizing battery life in photovoltaic systems," Florida Solar Energy Center / Sandia National Laboratories technical report.

S. Adhya, D. Saha, A. Das, J. Jana, and H. Saha, "An IoT based smart solar photovoltaic remote monitoring and control unit," in Proc. Int. Conf. Control, Instrumentation, Energy and Communication, 2016, pp. 432-436.

A. Priharti, A. F. K. Rosa, and D. Wijayanto, "IoT based photovoltaic monitoring system application," Journal of Physics: Conference Series, vol. 1367, 2019.

Espressif Systems, "ESP8266EX datasheet," vendor technical documentation.

Blynk Inc., "Blynk IoT platform documentation," vendor technical documentation.

A. A. Stonier, V. Arun, G. Peter, J. Jasmine, K. E. Vignesh, and B. Athish, "Level Shifted PWM Technique for Minimum Component Switched Capacitor Inverter," in Proc. 2024 International Conference on Advancements in Power, Communication and Intelligent Systems (APCI), 2024, doi: 10.1109/APCI61480.2024.10616899.

International Electrotechnical Commission, IEC 60904-3:2019, Photovoltaic devices - Part 3: Measurement principles for terrestrial photovoltaic solar devices with reference spectral irradiance data.

M. A. Green et al., "Solar cell efficiency tables (Version 67)," Progress in Photovoltaics: Research and Applications, 2026. Available: https://onlinelibrary.wiley.com/doi/abs/10.1002/pip.70068

Fraunhofer Institute for Solar Energy Systems ISE, Photovoltaics Report, updated July 2026. Available: https://www.ise.fraunhofer.de/en/publications/studies/photovoltaics-report.html